Cell

RyR1 S-Nitrosylation Underlies Environmental Heat Stroke and Sudden Death in Y522S RyR1 Knockin Mice

William J. Durham,[1,6] Paula Aracena-Parks,[1,6] Cheng Long,[1,6] Ann E. Rossi,[2] Sanjeewa A. Goonasekera,[2] Simona Boncompagni,[3] Daniel L. Galvan,[1] Charles P. Gilman,[1] Mariah R. Baker,[1] Natalia Shirokova,[4] Feliciano Protasi,[3] Robert Dirksen,[2] and Susan L. Hamilton[1,5,*]

[1]Department of Molecular Physiology and Biophysics, Baylor College of Medicine, Houston, TX 77030, USA

[2]Department of Pharmacology and Physiology, University of Rochester Medical Center, Rochester, NY 14642, USA

[3]Laboratory of Cellular Physiology, CeSI Centro Scienze dell'Invecchiamento, Università degli Studi G. d'Annunzio, Chieti, CH I-66013, Italy

[4]Department of Pharmacology and Physiology, UMDNJ, New Jersey Medical School, Newark, NJ 07103-2714, USA

[5]Present address: Department of Molecular Physiology and Biophysics, Baylor College of Medicine, One Baylor Plaza, 410B, Houston, TX 77030, USA.

[6]These authors contributed equally to this work.

*Correspondence: susanh@bcm.edu

DOI 10.1016/j.cell.2008.02.042

SUMMARY

Mice with a malignant hyperthermia mutation (Y522S) in the ryanodine receptor (RyR1) display muscle contractures, rhabdomyolysis, and death in response to elevated environmental temperatures. We demonstrate that this mutation in RyR1 causes Ca^{2+} leak, which drives increased generation of reactive nitrogen species (RNS). Subsequent *S*-nitrosylation of the mutant RyR1 increases its temperature sensitivity for activation, producing muscle contractures upon exposure to elevated temperatures. The Y522S mutation in humans is associated with central core disease. Many mitochondria in the muscle of heterozygous Y522S mice are swollen and misshapen. The mutant muscle displays decreased force production and increased mitochondrial lipid peroxidation with aging. Chronic treatment with *N*-acetylcysteine protects against mitochondrial oxidative damage and the decline in force generation. We propose a feed-forward cyclic mechanism that increases the temperature sensitivity of RyR1 activation and underlies heat stroke and sudden death. The cycle eventually produces a myopathy with damaged mitochondria.

INTRODUCTION

Heatstroke is a life-threatening illness characterized by elevated core body temperature (>40°C), leading to central nervous system and multiple organ dysfunction. Exertional or environmental heat stroke (EHS) is often triggered by strenuous exercise performed under hot and humid environmental conditions. However, some individuals are much more sensitive to EHS/sudden death, experiencing episodes under relatively mild environmental conditions. Sudden death in response to exertion or high environmental temperature in young, apparently fit adults such as athletes and military recruits can arise from pre-existing cardiac abnormalities (Thompson et al., 2007) or the acute onset of organ failure (e.g., heart, kidney, liver) (Bouchama and Knochel, 2002). However, death during exercise in warm environmental conditions could also arise from organ failure secondary to rhabdomyolysis of skeletal muscle. Consistent with this, exercise-induced sudden death has been reported in young healthy males with family histories of malignant hyperthermia (MH), a condition that predisposes individuals to rhabdomyolysis (Ellis et al., 1988; Pamukcoglu, 1988; Ryan and Tedeschi, 1997). MH is a life-threatening pharmacogenetic disorder caused by mutations in the skeletal muscle Ca^{2+} release channel (or ryanodine receptor, RyR1) characterized by episodes of uncontrolled muscle contracture triggered by halogenated anesthetics such as isoflurane or halothane (Jurkat-Rott et al., 2000; Lichtman and Oribabor, 2006; Treves et al., 2005).

Many similarities exist between EHS and MH. Two human RyR1 mutations (R401C and R614C) are associated with MH, EHS, and exercise-induced rhabdomyolysis (Davis et al., 2002; Wappler et al., 2001). MH and EHS share many common pathological features, including rhabdomyolysis, increases in serum creatine kinase, hyperkalemia, tachycardia, metabolic acidosis, and increased muscle production of inflammatory cytokines (Bouchama and Knochel, 2002; Ducreux et al., 2004), which are effects that can trigger kidney failure and cardiac arrhythmias. In addition, patients who have experienced heat stress are more likely to have MH-positive in vitro contracture tests, in which the contractile sensitivity of a muscle biopsy to triggering agents such as caffeine and halothane is enhanced (Bendahan et al., 2001; Hackl et al., 1991; Hopkins, 2000).

We (Chelu et al., 2006) recently created knockin mice with a mutation (Y522S) in RyR1, which, in humans, is associated

with MH, a high incidence of central cores, and type I fiber type predominance (Quane et al., 1994). Heterozygous mice ($RyR1^{Y522S/wt}$) are more sensitive to developing skeletal muscle contractures in response to caffeine treatment in vitro and to isoflurane inhalation in vivo, both hallmarks of MH. In addition, heat alone and/or exercise under warm conditions triggers rhabdomyolysis and death in $RyR1^{Y522S/wt}$ mice (Chelu et al., 2006). Although the mice undergo sustained whole body contractures upon heat exposure, death also frequently occurs in the absence of detectable sustained contractures. The molecular and cellular mechanisms whereby elevated temperatures with or without exercise leads to death of these mice are unknown. Here we demonstrate that enhanced Ca^{2+} leak from mutant RyR1 Ca^{2+} release channels increases oxidative/nitrosative stress, leading to *S*-nitrosylation of RyR1 that further enhances Ca^{2+} leak and increases susceptibility to heat-induced sudden death.

RESULTS

Heat Sensitivity of $RyR1^{Y522S/wt}$ Mice

$RyR1^{Y522S/wt}$ mice exposed to elevated environmental temperatures undergo an MH-like response characterized by rapid rhabdomyolysis and death (Chelu et al., 2006). Upon exposure to a 41°C heat challenge, the rectal temperature of anesthetized (non-triggering anesthetic etomidate) $RyR1^{Y522S/wt}$ mice increases more rapidly than in $RyR1^{wt/wt}$ mice (Figures 1A and 1B), suggesting that the mutant mice display enhanced metabolism and/or heat-induced muscle tension rapidly during heat exposure. Both enhanced metabolism and heat-induced muscle tension are likely to occur since (1) $RyR1^{Y522S/wt}$ mice exhibit a higher metabolic rate at 32°C than wild-type mice (Figure 1C), and (2) *solei* from $RyR1^{Y522S/wt}$ mice display increased basal stress at much lower temperatures than *solei* from wild-type animals (Figures 1D and 1E). Both enhanced metabolic rate and increased basal stress are likely to increase skeletal muscle production of reactive oxygen species (ROS) and reactive nitrogen species (RNS). To assess the role of ROS and RNS in the response of $RyR1^{Y522S/wt}$ mice to elevated temperatures, we tested the effects of treating mice for 3–5 days with either the antioxidant *N*-acetylcysteine (NAC, a precursor for glutathione synthesis) or the nitric oxide synthase (NOS) inhibitor, N (Ω)-nitro-L-arginine methyl ester (L-NAME). Both NAC and L-NAME delayed the rapid rise in core temperature in mutant mice (Figure 1B) and decreased the temperature sensitivity of basal tension of isolated *solei* (Figure 1E). NAC and L-NAME administered together did not improve the temperature response above either agent alone, and therefore combined treatment was not pursued further. NAC treatment reduces both ROS and RNS, and L-NAME prevents both RNS and ROS production by NOS (Clark et al., 2004; Pou et al., 1999), suggesting that either or both may be involved in the sensitization of $RyR1^{Y522S/wt}$ mice to temperature.

Oxidative/Nitrosative Stress in $RyR1^{Y522S/wt}$ Muscle

To assess oxidative/nitrosative stress in the muscle of the $RyR1^{Y522S/wt}$ mice, we measured levels of the primary intracellular antioxidant buffer glutathione (GSH), its oxidized form, glutathione disulfide (GSSG), and the GSH/GSSG ratio in skeletal muscle homogenates from mice not exposed to elevated temperatures. $RyR1^{Y522S/wt}$ muscle exhibits profound basal oxidative stress, with approximately a 50% reduction in both total GSH content (Figure S1) and the ratio GSH/GSSG (Figure 1F). A decreased GSH/GGSG ratio could reflect changes in ROS and/or RNS levels in muscle. Pretreatment of $RyR1^{Y522S/wt}$ mice with either NAC or L-NAME partially restores GSH levels and GSH/GSSG (Figure 1F), suggesting that part of the effect is due to RNS production.

To assess ROS and RNS production in myotubes derived from $RyR1^{Y522S/wt}$ mice, we used confocal imaging to compare, respectively, the fluorescence of 5-carboxy-2′,7′-dichlorodihydrofluorescein (DCF) and 4-amino-5-methylamino-2′,7′-difluorofluorescein (DAF) at room temperature and 37°C. In $RyR1^{Y522S/wt}$ myotubes, we found a significant temperature dependent increase in ROS (Figures 1G and 1H) and RNS (Figures 1I and 1J). Both increases in RNS and ROS are blocked by treatment with ryanodine and GSH ethyl ester (GSHEE), a membrane permeant form of glutathione (Figures 1G–1J). The ability of GSHEE to block temperature dependent increases in DAF fluorescence suggests that GSHEE treatment also reduces RNS. Importantly, L-NNA (N[Ω]-nitro-L-arginine), an inhibitor of nitric oxide synthase (NOS), blocks temperature-dependent increases in DAF fluorescence but does not significantly alter ROS production as assessed by DCF fluorescence (Figures 1G–1J). While L-NNA inhibits superoxide production by NOS (Clark et al., 2004), the absence of an inhibition of DCF fluorescence by L-NNA in our experiments suggests that DAF fluorescence in myotubes specifically reflects RNS production. Overall, these data demonstrate a temperature-dependent increase in both ROS and RNS production in $RyR1^{Y522S/wt}$ myotubes. Inhibition by ryanodine of the temperature-dependent increase in DCF and DAF fluorescence suggests that both ROS and RNS production are stimulated by RyR1-mediated Ca^{2+} release from the sarcoplasmic reticulum (SR). Two obvious questions arise from these studies: (1) Why is there increased ROS/RNS production with temperature in $RyR1^{Y522S/wt}$ myotubes, and (2) how do increased ROS/RNS levels relate to the enhanced temperature sensitivity of these mice?

Temperature-Dependent Increases in Resting Ca^{2+} Levels in Muscle of $RyR1^{Y522S/wt}$ Mice

To define the relationship between the mutation in RyR1 and increased oxidative/nitrosative stress, we determined the effects of temperature and antioxidants on resting Ca^{2+} levels in myotubes from $RyR1^{Y522S/wt}$ and $RyR1^{wt/wt}$ mice. We previously (Chelu et al., 2006) found enhanced caffeine sensitivity in $RyR1^{Y522S/wt}$ myotubes in the absence of a change in global resting Ca^{2+} levels at room temperature. However, the mutation in RyR1 is highly likely to produce local changes in Ca^{2+} that are rapidly sequestered back into the SR. We re-examined the effects of the Y522S mutation on Ca^{2+} homeostasis in myotubes (Figures 2A–2C) and muscle fibers (Figure 2D) at more physiological temperatures. Cytosolic Ca^{2+} levels increase with temperature to a much greater extent in $RyR1^{Y522S/wt}$ than in wild-type myotubes and muscle fibers (Figures 2A–2D). Figure 2C quantifies temperature-dependent changes in the intracellular concentration of free Ca^{2+} (in nM) in $RyR1^{wt/wt}$ and $RyR1^{Y522S/wt}$ myotubes. The lack of a statistically significant difference in

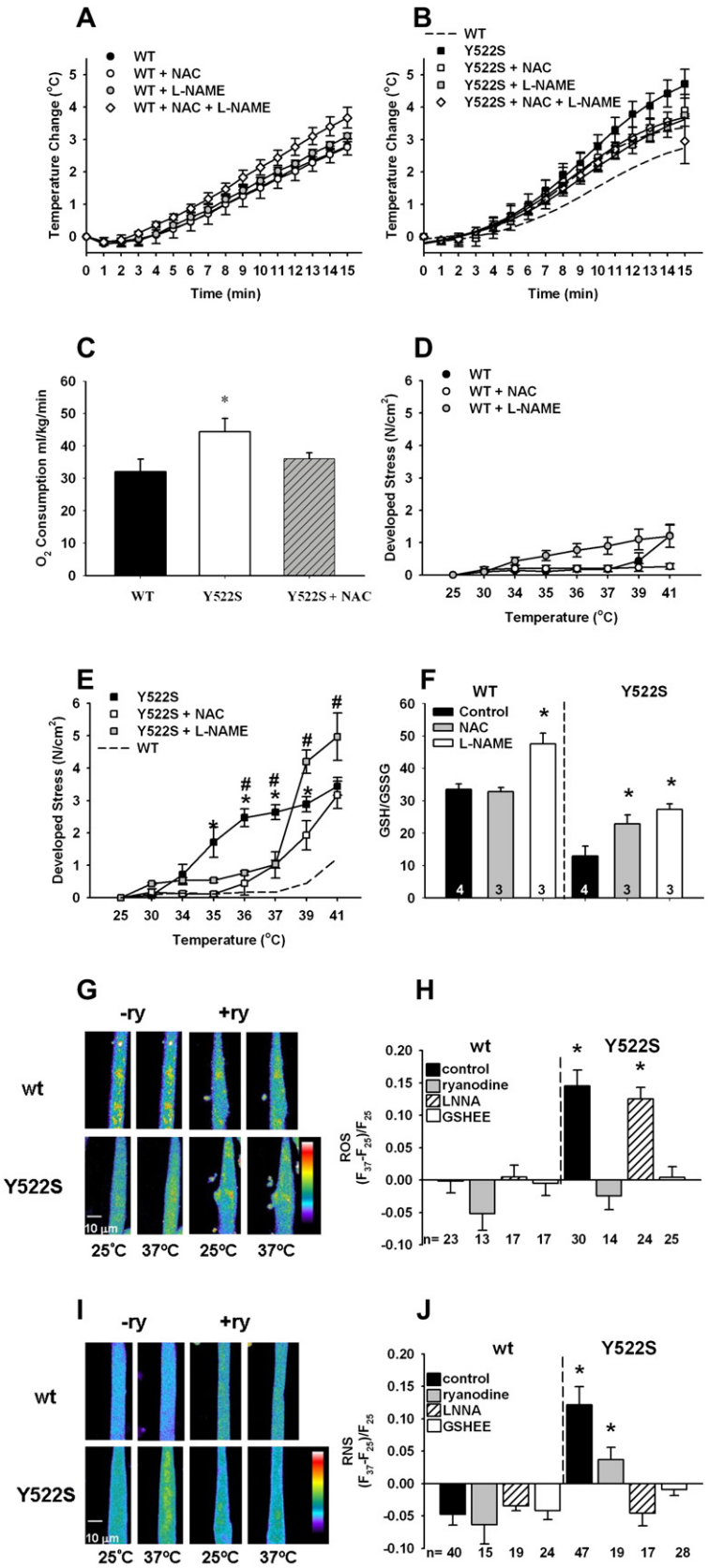

Figure 1. Effects of Warming on RyR1$^{Y522S/wt}$ Mice

(A) Rectal temperatures in RyR1$^{wt/wt}$ mice. Mice were anesthetized with etomidate (i.p.) and placed in an environmental chamber (41°C), and rectal temperatures were measured as a function of time in RyR1$^{wt/wt}$ mice (filled circles, n = 10) and in mice treated for 3–5 days with NAC (open circles, n = 6), L-NAME (gray circles, n = 4), or combined NAC and L-NAME (open diamonds, n = 4).

(B) Rectal temperatures in RyR1$^{Y522S/wt}$ mice. Similar measurements were made with RyR1$^{Y522S/wt}$ mice (filled squares, n = 7) and mice treated with NAC (open squares, n = 4), L-NAME (gray squares, n = 4), and combined NAC and L-NAME (open diamonds, n = 4). The dashed line represents the WT curve from Figure 1A for comparison. When the curves were compared by F tests, NAC ($p < 0.05$), L-NAME ($p < 0.001$), and NAC and L-NAME ($p < 0.001$) significantly attenuated the response versus no treatment in the RyR1$^{Y522S/wt}$ mice.

(C) VO_2 is increased at thermoneutral conditions in RyR1$^{Y522S/wt}$ mice. VO_2 was measured at 32°C using four to five mice in each group *$p < 0.05$ versus RyR1$^{wt/wt}$.

(D) Temperature sensitivity of basal stress in RyR1$^{wt/wt}$ *solei*. *Solei* from RyR1$^{wt/wt}$ (with and without prior treatment with NAC or L-NAME) were isolated, attached to force transducers, and heated progressively from an initial temperature of 25°C to 41°C. n = 3–8 mice/group.

(E) Temperature sensitivity of basal stress in RyR1$^{Y522S/wt}$ *solei*. Group, temperature, and interaction effects were significant ($p < 0.0001$) when data were analyzed by two-way ANOVA. *$p < 0.05$ to $p < 0.001$ RyR1$^{Y522S/wt}$ versus RyR1$^{Y522S/wt}$ NAC, #$p < 0.05$ to $p < 0.01$ RyR1$^{Y522S/wt}$ versus RyR1$^{Y522S/wt}$ L-NAME. For clarity, significant differences between L-NAME- and NAC-treated groups at 39°C and 41°C are not indicated on the graph.

(F) GSH/GSSG ratios. The data (n = 3–4) were compared between untreated mice of each genotype and the mice receiving the indicated treatment. *$p < 0.05$.

(G) Fluorescence imaging of myotubes loaded with DCF. All imaging data were obtained from multiple cells across at least three independent myotube preparations. Representative images obtained with DCF-loaded RyR1$^{wt/wt}$ and RyR1$^{Y522S/wt}$ myotubes at 25°C and 37°C in the presence and absence of ryanodine (20 µM).

(H) Changes in DCF fluorescence with temperature. ROS production was detected with DCF in the presence absence of ryanodine (20 µM), L-NNA (50 µM), and GSHEE (5 mM).

(I) Fluorescence imaging of myotubes loaded with DAF-AM. Representative images obtained with DAF-AM loaded RyR1$^{wt/wt}$ and RyR1$^{Y522S/wt}$ myotubes at 25°C and 37°C in the presence and absence of ryanodine (20 µM).

(J) Changes in DAF fluorescence with temperature. RNS production was detected with DAF in the presence or absence of ryanodine (20 µM), L-NNA (50 µM), and GSHEE (5 mM). All data in this figure are shown as mean ± SEM.

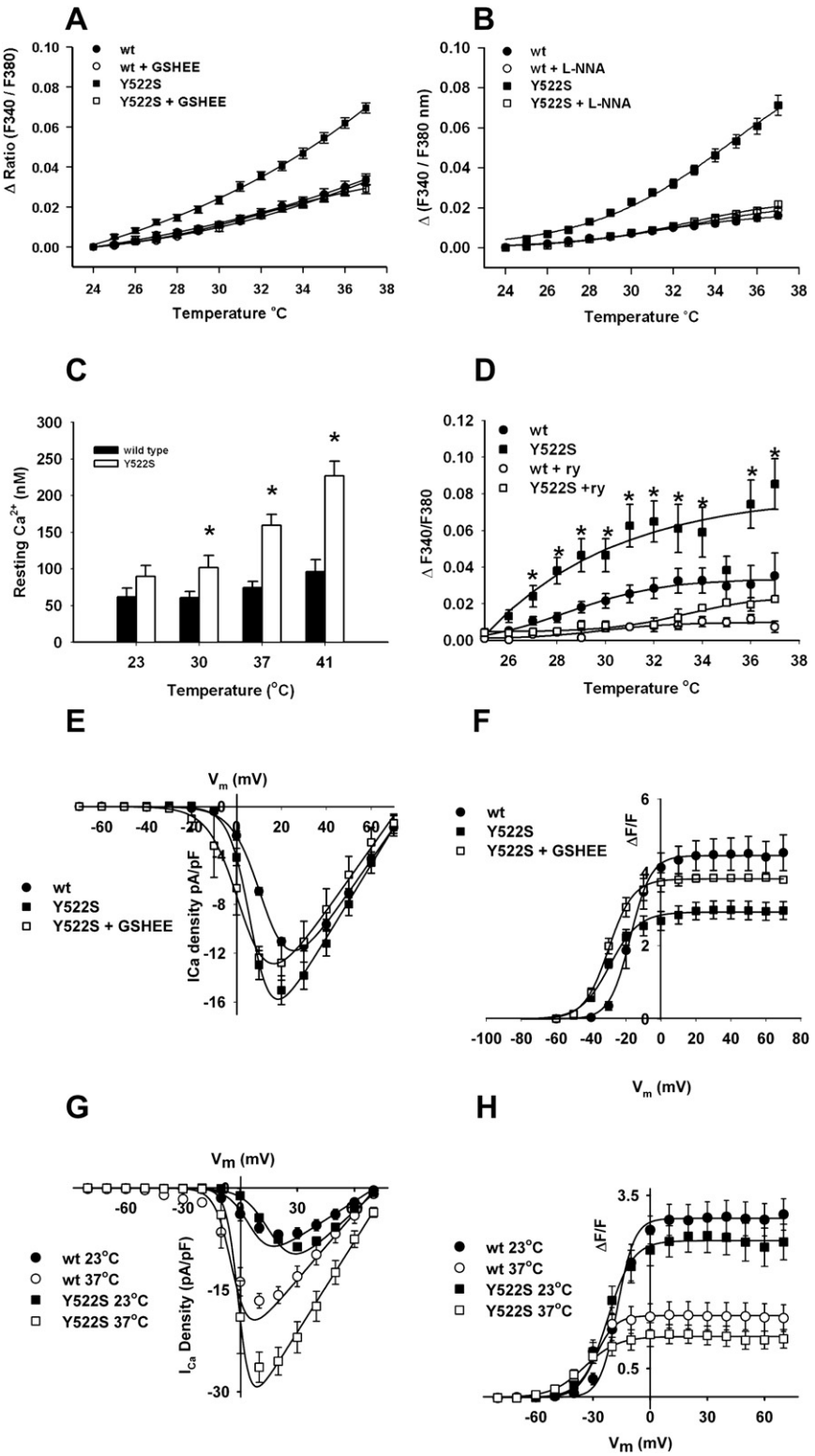

Figure 2. Temperature-Dependent Increases Cytosolic Ca^{2+} Levels in $RyR1^{Y522S/wt}$ Myotubes and *solei*

(A) Temperature-dependent increases in cytosolic Ca^{2+} levels measured with fura-2. Myotubes loaded with fura-2AM were warmed to the indicated temperatures in the presence and absence of 5mM GSHEE. Values are mean ± SEM for three independent cultures for each group: $RyR1^{wt/wt}$ (filled circles, n = 27), $RyR1^{wt/wt}$ + GSHEE (open circles, n = 31), $RyR1^{Y522S/wt}$ (filled squares, n = 29), $RyR1^{Y522S/wt}$ + GSHEE (open squares, n = 32) (*$p < 0.001$, F-test).

(B) Effect of L-NNA on temperature-dependent increase in resting Ca^{2+}. Myotubes loaded with fura-2AM were warmed to the indicated temperatures in the presence or absence of 50 μM L-NNA. $RyR1^{Y522S/wt}$ (filled squares, n = 27) $RyR1^{Y522S/wt}$ + L-NNA (open squares, n = 31), $RyR1^{wt/wt}$ (filled circles, n = 28), and $RyR1^{wt/wt}$ + L-NNA (open circles, n = 33) (*$p < 0.05$, F-test).

(C) Temperature-dependent increases in cytosolic free Ca^{2+} concentration in $RyR1^{Y522S/wt}$ myotubes. Indo-1-loaded myotubes were warmed to the indicated temperatures, and indo-1 ratios were calibrated as described in Experimental Procedures. *$p < 0.05$ compared to $RyR1^{wt/wt}$ at 23°C.

(D) Temperature-dependent increases in cytosolic Ca^{2+} in *solei* fibers. *Solei* fibers of $RyR1^{Y522S/wt}$ mice were loaded with fura-2 and resting Ca^{2+} was measured in the presence or absence of ryanodine (20 μM). $RyR1^{Y522S/wt}$ (filled squares, n = 17), $RyR1^{Y522S/wt}$ + 20 μM ryanodine (open squares, n = 10), $RyR1^{wt/wt}$ (filled circles, n = 12), and $RyR1^{wt/wt}$ + 20 μM ryanodine (open circles, n = 4). *$p < 0.05$, one-way ANOVA with posttests.

(E) Effects of GSHEE on the voltage dependence of L-type Ca^{2+} currents. Voltage dependence of average (± SEM) peak L-currents at room temperature in $RyR1^{wt/wt}$ myotubes (filled circles), $RyR1^{Y522S/wt}$ myotubes (filled squares), and $RyR1^{Y522S/wt}$ myotubes preincubated with 5 mM GSHEE (open squares).

(F) The effects of GSHEE on the voltage dependence of intracellular Ca^{2+} release. Ca^{2+} transients at room temperature were measured in $RyR1^{wt/wt}$ myotubes (filled circles), $RyR1^{Y522S/wt}$ myotubes (filled squares), and $RyR1^{Y522S/wt}$ myotubes preincubated with 5 mM GSHEE (open squares).

(G) Temperature dependence of L-type Ca^{2+} currents in $RyR1^{wt/wt}$ and $RyR1^{Y522S/wt}$ myotubes. Voltage dependence of average (± SEM) peak L-currents at 23°C (filled symbols) and 37°C (open symbols) in $RyR1^{wt/wt}$ myotubes (circles) and $RyR1^{Y522S/wt}$ (squares) myotubes. Each data set was fit (smooth, solid lines) using equations described previously (Chelu et al., 2006) in order to determine G_{max}, $V_{G1/2}$, k_G, and V_{rev} at both 23°C (167 nS/nF, 7.8 mV, 8.6 mV, and 72.6 mV for $RyR1^{wt/wt}$ and 242 nS/nF, 17.3, 7.1 mV, and 73.0 mV for $RyR1^{Y522S/wt}$, respectively) and 37°C (309 nS/nF, −3.0 mV, 7.0 mV, and 72.5 mV for $RyR1^{wt/wt}$ and 442 nS/nF, −0.6 mV, 4.5 mV, and 78.2 mV for $RyR1^{Y522S/wt}$, respectively).

(H) Temperature dependence of intracellular Ca^{2+} transients in $RyR1^{wt/wt}$ and $RyR1^{Y522S/wt}$ myotubes. Voltage dependence of average (± SEM) peak Ca^{2+} transient amplitude at 23°C (filled symbols) and 37°C (open symbols) in $RyR1^{wt/wt}$ myotubes (circles) and $RyR1^{Y522S/wt}$ (squares) myotubes Each data set was fit (smooth solid lines) using equations described previously (Chelu et al., 2006) in order to determine F_{max}, $V_{F1/2}$, and k_F at both 23°C (3.1, −16.8 mV, and

Table 1. Effects of GSHEE on E-C Coupling

Genotype	G_{max} (nS/nF)	k_G (mV)	$V_{G1/2}$ (mV)	V_{rev} (mV)	$(\Delta F/F)_{max}$	k_F (mV)	$V_{F1/2}$ (mV)
$RyR1^{wt/wt}$	264 ± 13	6.4 ± 0.2	12.8 ± 0.8	76.8 ± 1.7	4.5 ± 0.4	5.4 ± 0.84	−16.9 ± 1.4
	n = 6	n = 6	n = 6	n = 6	n = 6	n = 6	n = 6
$RyR1^{Y522S/wt}$	302 ± 22	4.7 ± 0.4	7.2 ± 0.7*	76.8 ± 2.9	2.9 ± 0.3*	8.5 ± 1.1	−29.0 ± 1.6*
	n = 7	n = 7	n = 7	n = 7	n = 7	n = 7	n = 7
$RyR1^{Y522S/wt}$ + 5mM GSHEE	266 ± 13	4.8 ± 0.2	1.3 ± 4.8	70.5 ± 4.6	3.9 ± 0.1	7.6 ± 1.6	−29.2 ± 1.4*
	n = 5	n = 5	n = 5	n = 5	n = 5	n = 5	n = 5

Values represent mean ± SEM for n number of experiments. Parameters for the voltage dependence of Ca^{2+} conductance and Ca^{2+} transients were obtained as previously described (Chelu et al., 2006). G_{max}, maximal L-channel conductance; $(\Delta F/F)_{max}$, maximal relative change in fluo-4 fluorescence; V_{rev}, L-channel reversal potential; $V_{G1/2}$ and $V_{F1/2}$, potential at which G and F are half maximal, respectively; k_G and k_F, slope factors for IV and FV, respectively. *$p < 0.01$ compared to $RyR1^{wt/wt}$.

cytosolic Ca^{2+} concentration at 23°C likely reflects the ability of SERCA to adequately resequester local increases in Ca^{2+} due to leak from the mutant RyR1 (i.e., compensated leak). Temperature-dependent increases in cytosolic Ca^{2+} are blocked by GSHEE (Figure 2A) and ryanodine. Elevations in resting Ca^{2+} increases are also blocked by both L-NNA (Figure 2B) and L-NAME (Figure S2), suggesting that the increases in cytosolic Ca^{2+} at higher temperatures are primarily attributable to increased RNS rather than ROS, since L-NNA only prevents temperature-dependent increases in RNS (Figures 1H and 1J).

We also examined the effects of the mutation on the magnitude, kinetics, and voltage dependence of L-type Ca^{2+} channel activity and SR Ca^{2+} release that occurs during excitation-contraction (E-C) coupling. For these experiments, myotubes derived from either $RyR1^{wt/wt}$ or $RyR1^{Y522S/wt}$ mice were incubated for 30 min in either vehicle or 5 mM GSHEE prior to perforated voltage-clamp recordings at room temperature (Figures 2E, 2F, and Figure S3A). Additional experiments were conducted to compare E-C coupling at room temperature (23°C) and 37°C (Figures 2G, 2H, and Figure S3B). Consistent with previous findings (Chelu et al., 2006), at 23°C L-current density is slightly larger in $RyR1^{Y522S/wt}$ myotubes (Figure 2E; Table 1) and the magnitude of Ca^{2+} release reduced and its voltage dependence shifted to more negative voltages in $RyR1^{Y522S/wt}$ myotubes (Figure 2F; Table 1). Preincubation of $RyR1^{Y522S/wt}$ myotubes with 5 mM GSHEE normalized peak L-current density and voltage-gated Ca^{2+} release without normalizing the voltage dependence of release (Figures 2E and 2F; Table 1). These results are consistent with increased oxidative/nitrosative stress in $RyR1^{Y522S/wt}$ myotubes reducing Ca^{2+} release during E-C coupling, but not in modulating the sensitivity of RyR1 to activation by the voltage sensor. The temperature dependence of representative L-type Ca^{2+} currents and intracellular Ca^{2+} transients in $RyR1^{wt/wt}$ and $RyR1^{Y522S/wt}$ myotubes are shown in Figure S3B. At 37°C, L-current magnitude is similarly increased and its kinetics of channel activation and inactivation accelerated in $RyR1^{wt/wt}$ and $RyR1^{Y522S/wt}$ myotubes. In addition, a similar reduction in voltage-gated Ca^{2+} release and hyperpolarization in the sensitivity of release is also observed in $RyR1^{wt/wt}$ and $RyR1^{Y522S/wt}$ myotubes at 37°C. The average voltage dependence of L-current density and intracellular Ca^{2+} transients are summarized in Figures 2G and 2H, respectively. Together, these data indicate that temperature has a similar effect on maximal Ca^{2+} channel conductance (G_{max} is increased about 180%) and voltage sensitivity of release ($V_{F1/2}$ is left-shifted ~13 mV) in both $RyR1^{wt/wt}$ and $RyR1^{Y522S/wt}$ myotubes, indicating that the EC coupling process in $RyR1^{wt/wt}$ and $RyR1^{Y522S/wt}$ myotubes is similarly affected by temperature. Thus, the increased temperature sensitivity observed $RyR1^{Y522S/wt}$ mice represents effects of temperature on the resting RyR1 channel and not the EC coupling process per se.

Effects of ROS/RNS Stress on RyR1 Channel Function in $RyR1^{Y522S/wt}$ Mice

Since RyR1 channel activation is increased by both oxidative/nitrosative modifications (Aghdasi et al., 1997; Marengo et al., 1998; Oba et al., 2002; Sun et al., 2003, 2001b), we compared the extent of RyR1 oxidative/nitrosative modifications using antibodies that are specific for either *S*-nitrosylation or *S*-glutathionylation in skeletal muscle SR membranes of $RyR1^{wt/wt}$ and $RyR1^{Y522S/wt}$ mice (Figures 3A and 3B). To normalize for differences in membrane preparation, we also western blotted with antibodies to RyR1. The use of antibodies to detect *S*-nitrosylation and *S*-glutathionylation with western blots was previously validated with the biotin switch in our laboratory (Aracena-Parks et al., 2006) and by mass spectrometric analyses of peptides labeled using the redox switch technology. We find significant increases in *S*-nitrosylation and *S*-glutathionylation of RyR1 in skeletal muscles of $RyR1^{Y522S/wt}$ mice (Figures 3A and 3B) that are eliminated by DTT. Ascorbic acid (AA) significantly reduces *S*-nitrosylation (Figure 3B) but not *S*-glutathionylation of RyR1 (Figure 3C). Oxidation of disulfides is also likely to occur, and we have previously detected a single intersubunit disulfide formed between subunits of the RyR1 tetramer (Zhang et al., 2003). We find no significant difference in the formation of this intersubunit crosslink in RyR1 between wild-type and mutant muscle (data not shown). We also compared the extent of *S*-nitrosylation and *S*-glutathionylation of RyR1 in mice treated for several days with either NAC or L-NAME. Both NAC and L-NAME prevent the increase in *S*-nitrosylation of the $RyR1^{Y522S/wt}$ (Figure 3B), while increased *S*-glutathionylation is decreased by NAC and abolished by L-NAME.

6.2 mV for $RyR1^{wt/wt}$ and 2.7, −23.1 mV, and 7.5 mV for $RyR1^{Y522S/wt}$, respectively) and 37°C (1.4, −31.8 mV, and 5.7 mV for $RyR1^{wt/wt}$ and 1.0, −35.6 mV, and 8.2 mV for $RyR1^{Y522S/wt}$, respectively for $RyR1^{Y522S/wt}$, respectively). All data in this figure are shown as mean ± SEM.

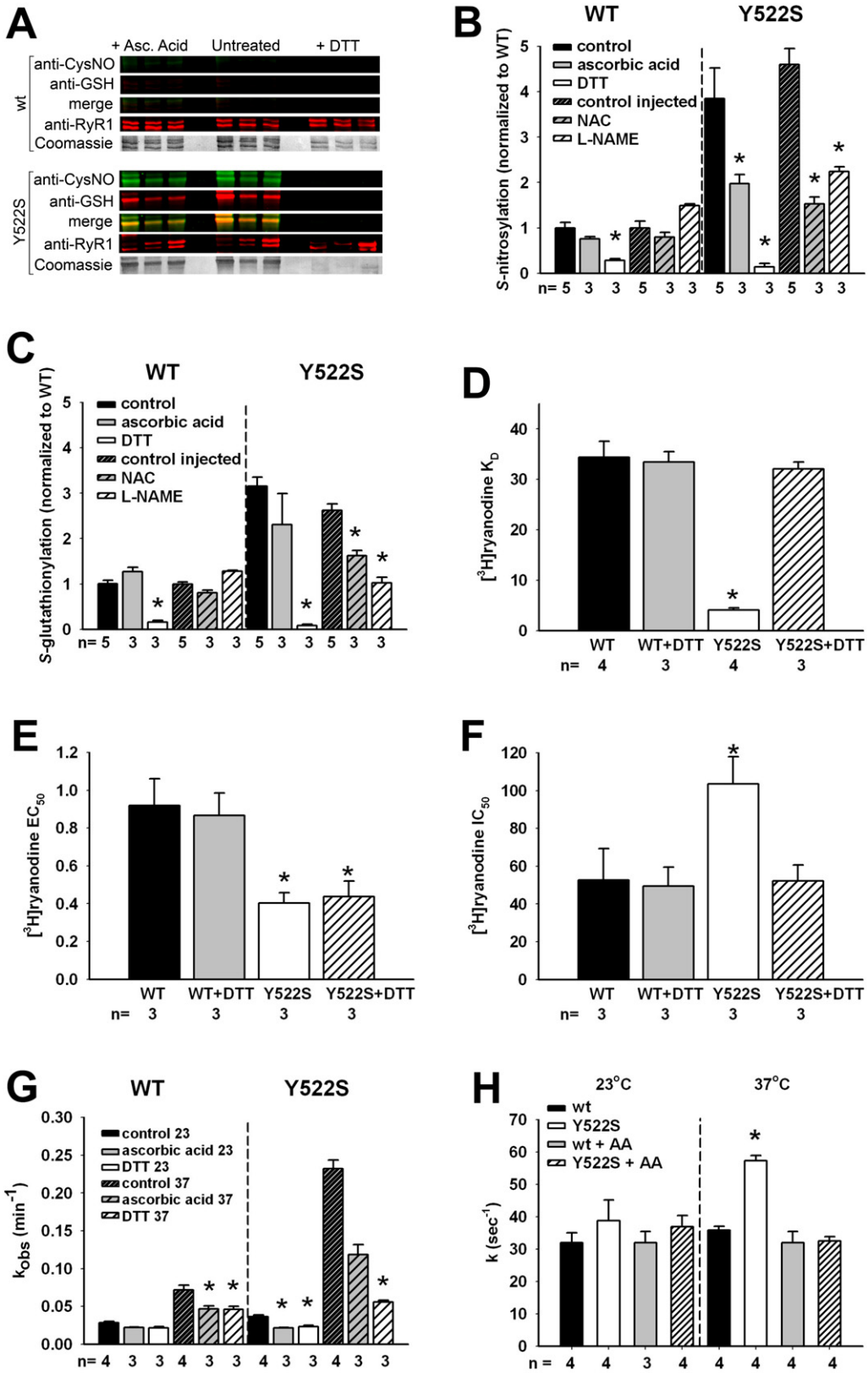
A
+ Asc. Acid
Untreated
+ DTT
wt
anti-CysNO
anti-GSH
merge
anti-RyR1
Coomassie
Y522S
anti-CysNO
anti-GSH
merge
anti-RyR1
Coomassie
B
WT
Y522S
control
ascorbic acid
DTT
control injected
NAC
L-NAME
S-nitrosylation (normalized to WT)
n= 5 3 3 5 3 3 5 3 3 5 3 3
C
WT
Y522S
control
ascorbic acid
DTT
control injected
NAC
L-NAME
S-glutathionylation (normalized to WT)
n= 5 3 3 5 3 3 5 3 3 5 3 3
D
[3H]ryanodine KD
WT
WT+DTT
Y522S
Y522S+DTT
n= 4 3 4 3
E
[3H]ryanodine EC50
WT
WT+DTT
Y522S
Y522S+DTT
n= 3 3 3 3
F
[3H]ryanodine IC50
WT
WT+DTT
Y522S
Y522S+DTT
n= 3 3 3 3
G
WT
Y522S
control 23
ascorbic acid 23
DTT 23
control 37
ascorbic acid 37
DTT 37
kobs (min-1)
n= 4 3 3 4 3 3 4 3 3 4 3 3
H
23°C
37°C
wt
Y522S
wt + AA
Y522S + AA
k (sec-1)
n = 4 4 3 4 4 4 4 4

Ryanodine binds preferentially to the RyR1 open state and is widely used to assess channel activity (Chu et al., 1990). We compared [^{3}H] ryanodine binding to membranes derived from RyR1$^{Y522S/wt}$ and RyR1$^{wt/wt}$ mice (Figures 3D–3H and S4–S6). The apparent K_D for [^{3}H] ryanodine binding is greatly decreased in SR membranes from RyR1$^{Y522S/wt}$ compared to RyR1$^{wt/wt}$ mice, and this difference is eliminated by DTT (Figure 3D and S4). Enhanced caffeine sensitivity, arising from an increased affinity of the activating site on RyR1 for Ca^{2+} (Pessah et al., 1987), is an inherent property of the mutant channel (Chelu et al., 2006). Consistent with this, RyR1 from RyR1$^{Y522S/wt}$ mice exhibits increased affinity for the Ca^{2+} activation site, and this increase in affinity is maintained in the presence of DTT (Figures 3E and S5). Thus, the Y522S mutation alters the intrinsic sensitivity of the channel to activators (e.g., caffeine, Ca^{2+}, voltage sensor), while the nitrosative modifications alter the sensitivity of the channel to temperature with little or no additional effect on its sensitivity to activators. The modifications also increase the IC_{50} for Ca^{2+} inhibition of [^{3}H] ryanodine binding to membranes from the muscle of RyR1$^{Y522S/wt}$ mice (Figures 3F and S5), suggesting that the redox-modified mutant channel remains open at Ca^{2+} concentrations that normally close the channel, thus contributing to increased Ca^{2+} leak.

The previously described binding assays were performed at room temperature. RyR1 is, however, not stable for extended periods of time at higher temperatures (Carroll et al., 1991), making equilibrium binding studies at physiologic temperatures difficult. To circumvent this problem, we assessed the rate of association of [^{3}H] ryanodine to skeletal muscle membranes from RyR1$^{Y522S/wt}$ and RyR1$^{wt/wt}$ mice at different temperatures and in the presence or absence of either DTT or AA. Representative association curves are shown in Figure S6, and the k_{obs} values are shown in Figure 3G. [^{3}H] ryanodine associates much more rapidly to muscle membranes from RyR1$^{Y522S/wt}$ mice than from RyR1$^{wt/wt}$ mice at 37°C. This difference is eliminated by DTT and significantly reduced by AA. Since AA does not significantly alter *S*-glutathionylation but reverses *S*-nitrosylation (Figures 3A–3C), these findings indicate that *S*-nitrosylation enhances the temperature sensitivity of RyR1. Our data further suggest that Ca^{2+} leak from the SR, arising from the Y522S mutation, increases RNS production that leads to subsequent *S*-nitrosylation of RyR1, which, in turn, further enhances Ca^{2+} leak and increases RyR1 sensitivity to activation by temperature. This results in a vicious feed-forward cycle in RyR1$^{Y522S/wt}$ mice, whereby Ca^{2+} leak increases RNS production and RNS production in turn potentiates increased Ca^{2+} leak at permissive temperatures.

To further demonstrate that the temperature-dependent effect on Ca^{2+} levels arises from *S*-nitrosylation of RyR1, we measured the rates of Ca^{2+} efflux from SR vesicles from RyR1$^{Y522S/wt}$ and RyR1$^{wt/wt}$ mice using stopped flow and Ca^{2+} Green 5N (Donoso et al., 2000), in the presence and absence of AA (Figure 3H). Figure S7 shows representative curves using SR vesicles from RyR1$^{Y522S/wt}$ and RyR1$^{wt/wt}$ membranes in the presence or absence of AA. Consistent with increased activity of the mutant channel, we found that the rate of Ca^{2+}-induced Ca^{2+} release (in the presence of 1 mM free ATP and 10 μM free Ca^{2+}) from RyR1$^{Y522S/wt}$ microsomes at 37°C was increased compared to RyR1$^{wt/wt}$ (Figure S7). The observed rate constants for Ca^{2+} efflux are shown in Figure 3H. The rate of Ca^{2+} efflux is significantly greater for RyR1$^{Y522S/wt}$ membranes at 37°C compared to that of RyR1$^{wt/wt}$ membranes, and this difference is eliminated by AA, indicating that the increased rate is due to RyR1 *S*-nitrosylation. Ryanodine (100 μM) completely blocks efflux in all conditions (data not shown).

Effects of the Y522S Mutation on Mitochondrial Structure and Muscle Function

The human Y522S mutation is associated with a myopathy characterized by central cores devoid of mitochondria. Prolonged Ca^{2+} leak combined with increased ROS/RNS production, such as that observed in RyR1$^{Y522S/wt}$ mice, is likely to impact the structure and function of closely apposed mitochondria, which could lead to altered muscle function. Using tetramethyl rhodamine ethylester (TMRE) to assess mitochondrial membrane potential, we found that TMRE fluorescence increases with temperature in RyR1$^{Y522S/wt}$ myotubes, but not in RyR1$^{wt/wt}$ myotubes (Figure S8), indicative of a hyperpolarization of the mitochondrial membrane potential. We also compared the ultrastructure of mitochondria in *flexor digitorum brevis* (*FDB*) and *soleus* muscle fibers from 2- to 3-month- and 1-year-old RyR1$^{wt/wt}$ and RyR1$^{Y522S/wt}$ mice. Most mitochondria in FDB fibers of

Figure 3. Redox Modifications of RyR1 and Functional Consequences

(A) Redox modifications of RyR1. Representative blots obtained with three independent microsomal preparations were obtained from RyR1$^{wt/wt}$ (top) and RyR1$^{Y522S/wt}$ (bottom) mice. Density of the bands corresponding to the redox modifications of RyR1 were obtained under control conditions (middle) or in the presence of either ascorbic acid (left) or DTT (right).

(B) Fluorescence signals for *S*-nitrosylation normalized to the Coomassie stain of each band. Data (mean ± SD, n = 3–5) are presented as the ratio to untreated microsomes. *$p < 0.05$ compared to control.

(C) Fluorescence signals for *S*-glutathionylation normalized to the Coomassie stain of each band. Data (mean ± SD, n = 3–5) are presented as the ratio to untreated microsomes. *$p < 0.05$ compared to control.

(D–F) Equilibrium [^{3}H] ryanodine binding. Scatchard plot analysis (see Figure S4) determination of K_D values for [^{3}H] ryanodine binding to microsomes from RyR1$^{wt/wt}$ and RyR1$^{Y522S/wt}$ muscle (D). [^{3}H] ryanodine binding was titrated at different Ca^{2+} concentrations to calculate EC_{50} (E) and IC_{50} (F) values from traces as those shown in Figure S5. *$p < 0.05$ compared to RyR1$^{wt/wt}$ or untreated controls.

(G) Temperature dependence of the association kinetics of [^{3}H] ryanodine binding. Microsomes from untreated mice were preincubated in vitro with buffer (untreated), AA or DTT as in (A). [^{3}H] ryanodine binding was assessed at different time points (1–90 min), and k_{obs} values (mean ± SD) were determined from three to four independent experiments. Statistical significance for all panels was obtained by two-way ANOVA. *$p < 0.05$ compared to RyR1$^{wt/wt}$ or untreated controls.

(H) Rate of Ca^{2+} efflux from SR vesicles. Ca^{2+}-induced Ca^{2+} release in the presence of 1 mM free ATP and 9–10 μM free Ca^{2+} was measured using stopped-flow spectrofluorometry. Ca^{2+} release was measured in RyR1$^{wt/wt}$ and RyR1$^{Y522S/wt}$ vesicles using extravesicular calcium green-5N under control conditions or following treatment with AA. Release rate constant values (k) were obtained by peak differential analysis of fluorescence data (representative traces shown in Figure S7). All data in this figure are shown as mean ± SEM.

wild-type mice are located circumferentially around the myofibrils at either side of the Z line in close proximity to the triads (Rossi et al., 2006). In sections that cut across the intermyofibrillar space, the mitochondria in muscle of the RyR1$^{wt/wt}$ mice are rounded or slightly elongated (Figure 4A, panels 1–3). The internal matrix is usually dark, and cristae appear well organized and parallel to one another. A very small percentage of mitochondria in the wild-type muscle are abnormal with "myelin figures" (Figure 4A, panel 4) or a somewhat disarranged external membrane and internal cristae (not shown), but are similar in size to the more typical mitochondria. In contrast, although typical mitochondria are also found (Figure 4B, panel 1), in FDB fibers of RyR1$^{Y522S/wt}$ mice a large number of mitochondria are abnormally shaped, swollen, and sometimes severely altered (Figure 4B, panels 2–4). The most noticeable changes include widening and loss of matrix density, an increase in overall size, loss/disorganization of the internal cristae (Figure 4B, panel 2), disruption of the external membrane (Figure 4B, panel 3 arrows), and vacuolization (stars in Figure 4B, panels 2 and 4). The number of severely disrupted mitochondria (such as those in Figure 4B, panels 2–4) varies significantly from fiber to fiber and sample to sample, but is always much higher in fibers from RyR$^{Y522S/wt}$ compared to RyR1$^{wt/wt}$ mice (9.1 versus 1.1%, Table 2, footnote a). The minimum mitochondrial diameter in RyR$^{wt/wt}$ and RyR$^{Y522S/wt}$ mice is about 30% larger ($p < 0.0001$) in fibers from RyR$^{Y522S/wt}$ mice, suggesting increased mitochondrial swelling (Table 2, footnote b). The mitochondria appear to be even more damaged at one year, but the nature of the damage varies greatly among muscle groups. In FDB and *soleus* muscles from 1-year-old RyR$^{Y522S/wt}$ mice, most mitochondria are severely swollen and disrupted (Figures 4D and 4F, stars). In contrast, in the muscle of RyR$^{wt/wt}$ mice, mitochondria are identical to those at 2 to 3 months of age, i.e., dark in appearance and small in size (Figures 4C and 4E, arrows). To more quantitatively evaluate the mitochondrial damage, we isolated samples enriched in mitochondria from the muscle of both 2- and 12-month-old RyR$^{wt/wt}$ and RyR$^{Y522S/wt}$ mice. Mitochondrial content of the samples was confirmed as a >100-fold enrichment of succinate dehydrogenase (SDH) activity compared to homogenates (not shown). We measured the level of thiobarbituric acid-reactive substances (TBARS) as a marker of lipid peroxidation (i.e., oxidative damage) of mitochondrial membranes. Consistent with the mitochondrial damage observed in electron-microscopic (EM) analyses, an increase in lipid peroxidation is observed in mitochondria isolated from 2-month-old RyR1$^{Y522S/wt}$ mice compared to RyR1$^{wt/wt}$ mitochondria (Figure 4G), and this is substantially greater at 12 months. To determine if this arises from increased oxidative/nitrosative stress, we treated mice with NAC in their water supply for several months prior to sacrifice and mitochondrial isolation from pooled skeletal muscles. As can be seen in Figure 4G, NAC treatment completely reversed the increased mitochondrial lipid peroxidation observed in RyR1$^{Y522S/wt}$ mice.

To assess the functional consequences of aging under conditions of chronic oxidative/nitrosative stress in muscle of RyR1$^{Y522S/wt}$ mice, we measured the ability of the *soleus* muscle to generate force and found that the muscles from older ($\geq$8-month-old) RyR1$^{Y522S/wt}$ mice display a significant decrease in maximal developed force, and this decrease is prevented by chronic administration of NAC in their water supply (Figures 4H and 4I).

Our findings are consistent with mitochondrial damage resulting from prolonged oxidative/nitrosative stress contributing to contractile dysfunction in aged RyR1$^{Y522S/wt}$. However, SR Ca^{2+} leak and store depletion could also directly impact muscle function. We find that maximal caffeine induced stress is reduced in the RyR1$^{Y522S/wt}$ mice, and this is also prevented by chronic feeding of NAC to the mice in their drinking water (Figure 4J). The observed reduction in maximal caffeine-induced contracture could result from a decrease in releasable Ca^{2+} stores, reduced myofilament Ca^{2+} sensitivity, or both.

DISCUSSION

Environmental heat stress triggers sudden death in RyR1$^{Y522S/wt}$ mice. We suggest that this is due to a cycle whereby elevated cytosolic Ca^{2+}, combined with temperature-dependent increases in RNS, produce nitrosative modifications of the mutant channel that enhance RyR1 channel activity at elevated temperatures. The net result is a destructive feed-forward cycle of increased myoplasmic Ca^{2+} and RNS with temperature (Figure 5), ultimately producing EHS in RyR1$^{Y522S/wt}$ mice. Over an extended period, this cycle appears to produce a myopathy characterized by decreased force generation and damaged mitochondria.

RyR1 blockers, ROS/RNS scavengers, and inhibitors of NOS abolish temperature-dependent increases in cytosolic Ca^{2+} and RNS. Since NOS inhibition blocks temperature-dependent increases in Ca^{2+} and RNS, but not ROS, these results suggest that the increase in Ca^{2+} results from the increase in RNS. We do not know which NOS isoform(s) is involved, but skeletal muscle is rich in nNOS and this isoform may be activated by increases in cytosolic Ca^{2+}, since it colocalizes with ryanodine receptors in cardiac myocytes (Barouch et al., 2002; Hare, 2003). Although most nNOS localizes to the sarcolemma in skeletal muscle (Wells et al., 2003), close juxtapositioning of RyR1 and a subpopulation of nNOS in the triad junction might allow for a very local RyR1-mediated Ca^{2+} leak from RyR1 to stimulate NO production by nNOS.

We previously identified seven specific cysteines in one subunit of RyR1 (out of 100) that can be *S*-nitrosylated (Aracena-Parks et al., 2006). Of these, four (C315, C811, C906, and C3635) are endogenously nitrosylated. Stamler and coworkers (Eu et al., 2000; Sun et al., 2001a, 2003, 2001b) found that C3635 is the primary RyR1 cysteine that is *S*-nitrosylated at low pO_2. At high pO_2, some cysteines (not C3635) are oxidized, preventing RyR1 *S*-nitrosylation (Sun et al., 2003). Thus, C3635 is the best candidate for *S*-nitrosylation of RyR1$^{Y522S/wt}$ in our mice, and studies are currently ongoing to determine if nitrosylation of this residue in necessary and sufficient for enhancing RyR1 temperature sensitivity.

The Y522S mutation in humans is associated with a myopathy and central cores in muscle fibers. Although we did not detect widespread central cores in our mice, young mice displayed evidence of a myopathy in terms of mitochondrial alterations, while muscle function is not greatly compromised. In contrast, older RyR1$^{Y522S/wt}$ *solei* display marked mitochondrial structural damage and a decreased ability to generate force that is prevented

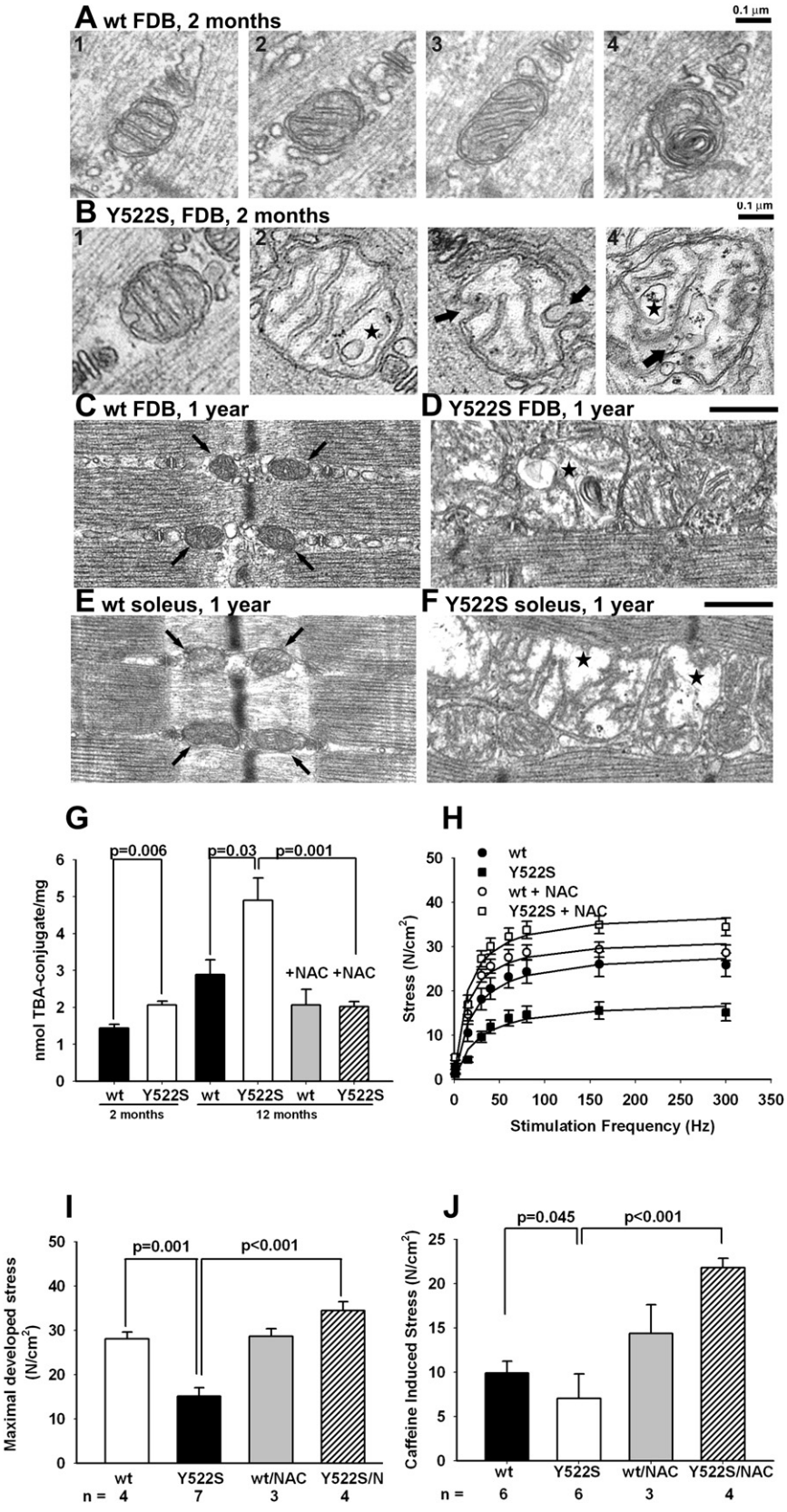

Figure 4. Effects of the Y522S Mutation on Mitochondrial Structure and Muscle Function

(A–F) Mitochondrial ultrastructure is altered in muscle of RyR1$^{Y522S/wt}$ mice. In (A), mitochondria of RyR1$^{wt/wt}$ fibers at 2–3 months of age are usually regularly shaped, appearing either round (panels 1 and 2) or slightly elongated (panel 3), with a dark/dense internal matrix. Abnormal mitochondria (panel 4) are rare in RyR1$^{wt/wt}$ fibers. (B). In RyR1$^{Y522S/wt}$ fibers, some normal mitochondria are present (panel 1), but abnormal mitochondria are frequent (panels 2–4). In (C)–(F), at 1 year, a much larger percentage of mitochondria are severely swollen/disrupted than at 2–3 months of age in both in FDB and *soleus* muscles from RyR1$^{Y522S/wt}$ mice (D and F, stars). In wt FDB (C) and *soleus* (E) muscles, on the other hand, mitochondria appear similar to those at 2–3 month of age.

(G) Mitochondrial lipid peroxidation in young and aged mice. Mitochondrial enriched fractions from 2- or 12-month-old mice with or without chronic NAC-treatment (≥2 months) were isolated and TBARS were measured in acid supernatants after protein precipitation, as detailed in Experimental Procedures. Shown are the mean of three independent determinations ± SD.

(H–J) Effect of chronic NAC treatment on skeletal muscle function of aged mice. Male RyR1$^{wt/wt}$ and RyR1$^{Y522S/wt}$ mice (≥1 year old) were treated with NAC (1% w/v) in their drinking water for at least 2 months prior to sacrifice. *Solei* were removed and stimulated in vitro, as described in Experimental Procedures. Shown are data for stress developed at increasing frequency of electrical stimulation (H) and the maximal tension per cross-sectional area obtained by maximal electrical stimulation (I) or application of 20 mM caffeine (J). All data in this figure are shown as mean ± SEM.

Table 2. EM Examination Reveals Frequent Severely Disrupted and Larger Mitochondria in Y522S Fibers

Genotype/ Age	Percentage of Severely Disrupted Mitochondria[a]	Average Diameter of Mito, nm ± SD[b]
$RyR1^{wt/wt}$ (2–3 months)	1.1 (n = 1019, 2 mice)	187 ± 53 (n = 643, 2 mice)
$RyR1^{Y522S/wt}$ (2–3 months)	9.1* (n = 1493, 4 mice)	243 ± 72* (n = 1069, 4 mice)

[a] The relative percentage of severely disrupted mitochondria in FDB fibers from 2- to 3-month-old $RyR1^{wt/wt}$ and $RyR1^{Y522S/wt}$ mice. n, total number of mitochondria.

[b] Differences in mitochondria mean diameter in FDB fibers from $RyR1^{wt/wt}$ and $RyR1Y^{522S/wt}$ mice. n, number of measurements. (*$p < 0.0001$). Data are mean ± SD.

by treating the mice with NAC. Mitochondrial lipid peroxidation is greatly increased in the muscle of older $RyR1^{Y522S/wt}$ mice, and this is also prevented by NAC. Thus, chronic exposure to elevated Ca^{2+} and ROS/RNS leads to progressive mitochondrial damage and decreased ability to generate force, suggesting that these pathways contribute to the myopathy observed in older mice.

The temperature and exercise sensitivity of $RyR1^{Y522S/wt}$ mice provide new mechanistic insight into environmental and/or exertional heat illness, disorders that have previously been linked in humans to MH mutations in RyR1 (Davis et al., 2002; Wappler et al., 2001). Consistent with this linkage, the probability of an MH response to exercise or volatile anesthetics in $RyR1^{Y522S/wt}$ mice is decreased by cooling (data not shown). Recent evidence indicates that intensive exercise also promotes RyR1 *S*-nitrosylation (Bellinger et al., 2008). Our data demonstrate that exercise, EHS, and heat-induced sudden death can result from a disease mutation in RyR1 that promotes Ca^{2+} leak, enhances nitrosative stress, and promotes subsequent *S*-nitrosylation of the mutant RyR1. It remains to be determined if EHS in humans is caused by RyR1 mutations that promote a similar

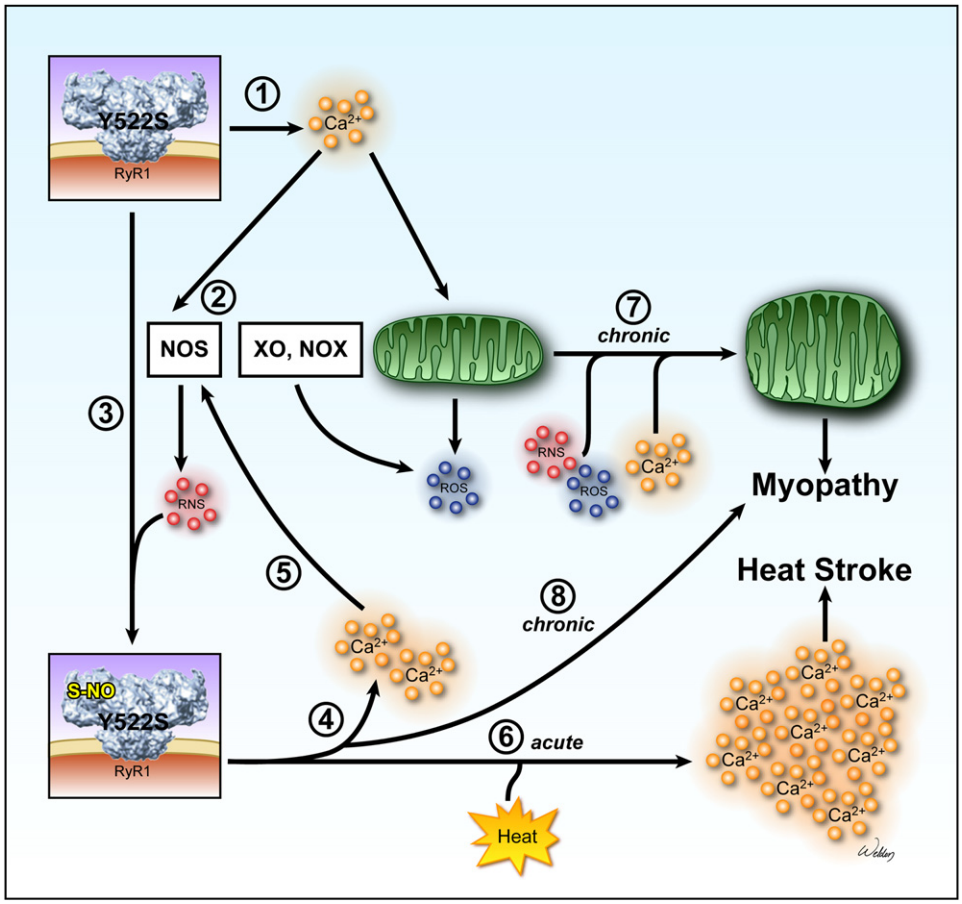

Figure 5. Proposed Model of Exertional/Environmental Heat Stress and Myopathy in $RyR1^{Y522S/wt}$ Mice

(1) SR Ca^{2+} release channels in $RyR1^{Y522S/wt}$ mice are more sensitive to voltage, ligand, and Ca^{2+} activation and open more readily, producing small, possibly local, increases in resting Ca^{2+}. (2) Increased cytosolic Ca^{2+} levels enhance ROS/RNS production. Increases in RNS are likely to be produced by nitric oxide synthases (NOS). Possible sources of ROS include mitochondria, xanthine oxidase (XO), and NAD(P)H oxidases (NOX). (3) Although both *S*-glutathionylation and *S*-nitrosylation of $RyR1^{Y522S/wt}$ occur, our data suggest that *S*-nitrosylation alone enhances the temperature sensitivity of RyR1. (4) *S*-nitrosylation of $RyR1^{Y522S/wt}$ increases its sensitivity to temperature and decreases its sensitivity to Ca^{2+} inhibition further promoting SR Ca^{2+} leak. (5) Ca^{2+} increases further enhance ROS/RNS production. (6) In response to heat stress, Ca^{2+} release from the modified $RyR1^{Y522S/wt}$ is greatly and persistently augmented, leading to heat stroke. (7 and 8) Chronically elevated levels of Ca^{2+} and ROS/RNS damage mitochondria and contribute to the development of myopathy.

feed-forward mechanism of uncontrolled Ca^{2+} leak and nitrosative stress.

In summary, our data demonstrate that Ca^{2+} release channels in $RyR1^{Y522S/wt}$ mice are leaky, producing elevations in resting Ca^{2+}, ROS, RNS, and basal stress at physiologically relevant temperatures. Our data support the involvement of a destructive feed-forward cycle whereby Ca^{2+} leak enhances RNS production, and subsequent *S*-nitrosylation of RyR1 further increases Ca^{2+} leak, resulting in regenerative Ca^{2+} release that underlies uncontrolled contractions during heat stress. We also suggest that increased Ca^{2+}, RNS, and/or ROS ultimately contribute to the progressive development of a myopathy characterized by decreased muscle performance and mitochondrial damage. An intriguing aspect of this study is the possibility that RyR1 mutations together with nitrosative stress represent a "double-hit mechanism" that underlies a subset of human cases of enhanced susceptibility to heat stroke, exertional/environmental illness, and/or sudden death.

EXPERIMENTAL PROCEDURES

Mice

All procedures were approved by the IACUC at Baylor College of Medicine and UCAR at the University of Rochester. For in vivo antioxidant treatment, mice were provided *ad libitum* access to drinking water containing NAC (1% w/v), L-NAME (1% w/v), or NAC plus L-NAME (both at 1% w/v).

In Vivo Temperature Sensitivity

Mice were anesthetized with etomidate, which does not trigger MH episodes in either MH susceptible humans (Robertson, 1992) or $RyR1^{Y522S/wt}$ mice. Two minutes following etomidate injection, mice were placed in an environmental chamber at 41°C. The initial core body temperature, as well as the temperature every minute thereafter, was monitored over the next 15 min of exposure.

Contractile Studies

Muscle collection and contractile studies were performed as previously described (Chelu et al., 2006). For determination of maximal developed stress, the data were fitted to a sigmoidal curve with the peak value of this curve reported as the maximal stress.

Isolation of Subcellular Fractions from Mouse Skeletal Muscle

Muscle from each mouse was quickly collected, snap frozen in liquid nitrogen, and stored at −80°C for up to 2 weeks. Microsomes or mitochondrial-enriched samples were obtained from thawed muscle by differential centrifugation (see Supplemental Data).

Ca^{2+} Flux Studies

Microsomal vesicles (1mg/ml) from $RyR1^{wt/wt}$ or $RyR1^{Y522S/wt}$ skeletal muscle were passively loaded with Ca^{2+}, and Ca^{2+} release kinetics was analyzed at 25°C, as described previously (Donoso et al., 2000), using a KinTek SF-2002 thermoregulated stopped-flow spectrometer (KinTek Corporation). Studies at 37°C were performed after 5 min equilibration of samples in the equipment. Release rate constants were obtained from peak differential analysis of raw fluorescence data.

Lipoperoxidation Assay

Basal lipoperoxidation levels were measured using thiobarbituric acid reactive substances (TBARS) as described elsewhere (Letelier et al., 2005).

Glutathione Assays

Total GSH and GSSG were assayed using deproteinized muscle homogenates in a 96-well format according to Tietze (Tietze, 1969), as modified by Griffith (Griffith, 1980).

Primary Cultures and Fluorescent Microscopy

Primary myotube cultures were grown on Matrigel (BD Biosciences) coated glass coverslips from 1- to 4-day-old mice as previously described (Pollard and Walker, 1997). ROS and RNS imaging were performed using the probes DCF or DAF, as detailed in Supplemental Experimental Procedures. Ca^{2+} imaging was performed as previously described in Long et al. (2007). Perforated patch clamp recordings of L-type Ca^{2+} currents (L-currents), and intracellular Ca^{2+} transients were recorded as described in Chelu et al. (2006). Details are described in Supplemental Experimental Procedures.

Western Blotting

Western blotting with mouse anti-glutathione 1:10,000 (Virogen) and rabbit anti-S-nitrosocysteine 1:10,000 (Sigma) were performed and analyzed as previously described (Aracena-Parks et al., 2006). Stripping of membranes was performed with Li-COR Stripping Solution, following the manufacturer's directions. Stripped membranes were reprobed with a mouse anti-RyR1 1:10,000 (Affinity Bioreagents), only to confirm the identity of the analyzed band. This antibody displays different affinities for RyR1 electrophoresed under reducing or nonreducing conditions. Thus, fluorescent data were normalized to the Coomasie stain of the blots.

[^{3}H] Ryanodine Binding

Equilibrium binding was performed with microsomes as detailed previously (Aracena-Parks et al., 2006). Ca^{2+} titration of binding was performed with 5 nM [^{3}H] ryanodine as described by Rodney et al. (2000). Kinetic assays with 5 nM [^{3}H] ryanodine at 23°C or 37°C were measured as detailed in Hawkes et al. (1992). Details of buffers used can be found in Supplemental Experimental Procedures.

Preparation and Analysis of Samples for EM

EM was performed in FDB and soleus muscles from 2- to 3-month- and 1 year-old mice as detailed in Paolini et al. (2007). Details are described in Supplemental Experimental Procedures.

Statistical Analyses

All analyses were performed in Sigma Plot (Systat Software, Incorporated).

SUPPLEMENTAL DATA

Supplemental data include eight figures, Supplemental Experimental Procedures, and Supplemental References and can be found with this article online at http://www.cell.com/cgi/content/full/133/1/53/DC1/.

ACKNOWLEDGMENTS

This work was supported by grants from NIH (AR 050503 and AR053349 to S.L.H., AR44657 to R.T.D., and 5P01AR052354 to S.L.H. and R.T.D.), the Muscular Dystrophy Association to S.L.H, Research Grant GGP030289 from the Italian Telethon Foundation to F.P, and a NIH Dental and Craniofacial training grant T32-DE07202 to A.E.R.

Received: July 5, 2007
Revised: October 30, 2007
Accepted: February 29, 2008
Published: April 3, 2008

REFERENCES

Aghdasi, B., Reid, M.B., and Hamilton, S.L. (1997). Nitric oxide protects the skeletal muscle Ca^{2+} release channel from oxidation induced activation. J. Biol. Chem. *272*, 25462–25467.

Aracena-Parks, P., Goonasekera, S.A., Gilman, C.P., Dirksen, R.T., Hidalgo, C., and Hamilton, S.L. (2006). Identification of cysteines involved in S-nitrosylation, S-glutathionylation, and oxidation to disulfides in ryanodine receptor Type 1. J. Biol. Chem. *281*, 40354–40368.

Barouch, L.A., Harrison, R.W., Skaf, M.W., Rosas, G.O., Cappola, T.P., Kobeissi, Z.A., Hobai, I.A., Lemmon, C.A., Burnett, A.L., O'Rourke, B., et al. (2002). Nitric oxide regulates the heart by spatial confinement of nitric oxide synthase isoforms. Nature *416*, 337–339.

Bellinger, A.M., Reiken, S., Dura, M., Murphy, P.W., Deng, S.X., Landry, D.W., Nieman, D., Lehnart, S.E., Samaru, M., Lacampagne, A., and Marks, A.R. (2008). Remodeling of ryanodine receptor complex causes "leaky" channels: a molecular mechanism for decreased exercise capacity. Proc. Natl. Acad. Sci. USA *105*, 2198–2202.

Bendahan, D., Kozak-Ribbens, G., Confort-Gouny, S., Ghattas, B., Figarella-Branger, D., Aubert, M., and Cozzone, P.J. (2001). A noninvasive investigation of muscle energetics supports similarities between exertional heat stroke and malignant hyperthermia. Anesth. Analg. *93*, 683–689.

Bouchama, A., and Knochel, J.P. (2002). Heat stroke. N. Engl. J. Med. *346*, 1978–1988.

Carroll, S., Skarmeta, J.G., Yu, X., Collins, K.D., and Inesi, G. (1991). Interdependence of ryanodine binding, oligomeric receptor interactions, and Ca^{2+} release regulation in junctional sarcoplasmic reticulum. Arch. Biochem. Biophys. *290*, 239–247.

Chelu, M.G., Goonasekera, S.A., Durham, W.J., Tang, W., Lueck, J.D., Riehl, J., Pessah, I.N., Zhang, P., Bhattacharjee, M.B., Dirksen, R.T., and Hamilton, S.L. (2006). Heat- and anesthesia-induced malignant hyperthermia in an RyR1 knock-in mouse. FASEB J. *20*, 329–330.

Chu, A., Diaz-Munoz, M., Hawkes, M.J., Brush, K., and Hamilton, S.L. (1990). Ryanodine as a probe for the functional state of the skeletal muscle sarcoplasmic reticulum Ca^{2+}release channel. Mol. Pharmacol. *37*, 735–741.

Clark, C.B., Zhang, Y., Martin, S.M., Davies, L.R., Xu, L., Kregel, K.C., Miller, F.J., Buettner, G.R., and Kerber, R.E. (2004). The nitric oxide synthase inhibitor N(omega)-nitro-L-arginine decreases defibrillation-induced free radical generation. Resuscitation *60*, 351–357.

Davis, M., Brown, R., Dickson, A., Horton, H., James, D., Laing, N., Marston, R., Norgate, M., Perlman, D., Pollock, N., and Stonwell, K. (2002). Malignant hyperthermia associated with exercise-induced rhabdomyolysis or congenital abnormalities and a novel RYR1 mutation in new zealand and australian pedigrees. Br. J. Anaesth. *88*, 508–515.

Donoso, P., Aracena, P., and Hidalgo, C. (2000). Sulfhydryl oxidation overrides $mg(^{2+})$ inhibition of calcium-induced calcium release in skeletal muscle triads. Biophys. J. *79*, 279–286.

Ducreux, S., Zorzato, F., Muller, C., Sewry, C., Muntoni, F., Quinlivan, R., Restagno, G., Girard, T., and Treves, S. (2004). Effect of ryanodine receptor mutations on interleukin-6 release and intracellular calcium homeostasis in human myotubes from malignant hyperthermia-susceptible individuals and patients affected by central core disease. J. Biol. Chem. *279*, 43838–43846.

Ellis, F.R., Halsall, P.J., and Harriman, D.G. (1988). Malignant hyperpyrexia and sudden infant death syndrome. Br. J. Anaesth. *60*, 28–30.

Eu, J.P., Sun, J., Xu, L., Stamler, J.S., and Meissner, G. (2000). The skeletal muscle calcium release channel: coupled o_2 sensor and no signaling functions. Cell *102*, 499–509.

Griffith, O.W. (1980). Determination of glutathione and glutathione disulfide using glutathione reductase and 2-vinylpyridine. Anal. Biochem. *106*, 207–212.

Hackl, W., Winkler, M., Mauritz, W., Sporn, P., and Steinbereithner, K. (1991). Muscle biopsy for diagnosis of malignant hyperthermia susceptibility in two patients with severe exercise-induced myolysis. Br. J. Anaesth. *66*, 138–140.

Hare, J.M. (2003). Nitric oxide and excitation-contraction coupling. J. Mol. Cell. Cardiol. *35*, 719–729.

Hawkes, M.J., Nelson, T.E., and Hamilton, S.L. (1992). [3H] ryanodine as a probe of changes in the functional state of the ca^{2+} -release channel in malignant hyperthermia. J. Biol. Chem. *267*, 6702–6709.

Hopkins, P.M. (2000). Malignant hyperthermia: advances in clinical management and diagnosis. Br. J. Anaesth. *85*, 118–128.

Jurkat-Rott, K., McCarthy, T., and Lehmann-Horn, F. (2000). Genetics and pathogenesis of malignant hyperthermia. Muscle Nerve *23*, 4–17.

Letelier, M.E., Lepe, A.M., Faundez, M., Salazar, J., Marin, R., Aracena, P., and Speisky, H. (2005). Possible mechanisms underlying copper-induced damage in biological membranes leading to cellular toxicity. Chem. Biol. Interact. *151*, 71–82.

Lichtman, A.D., and Oribabor, C. (2006). Malignant hyperthermia following systemic rewarming after hypothermic cardiopulmonary bypass. Anesth. Analg. *102*, 372–375.

Long, C., Cook, L.G., Hamilton, S.L., Wu, G.Y., and Mitchell, B.M. (2007). FK506 binding protein 12/12.6 depletion increases endothelial nitric oxide synthase threonine 495 phosphorylation and blood pressure. Hypertension *49*, 569–576.

Marengo, J.J., Hidalgo, C., and Bull, R. (1998). Sulfhydryl oxidation modifies the calcium dependence of ryanodine-sensitive calcium channels of excitable cells. Biophys. J. *74*, 1263–1277.

Oba, T., Murayama, T., and Ogawa, Y. (2002). Redox states of type 1 ryanodine receptor alter Ca(2+) release channel response to modulators. Am. J. Physiol. Cell Physiol. *282*, C684–C692.

Pamukcoglu, T. (1988). Sudden death due to malignant hyperthermia. Am. J. Forensic Med. Pathol. *9*, 161–162.

Paolini, C., Quarta, M., Nori, A., Boncompagni, S., Canato, M., Volpe, P., Allen, P.D., Reggiani, C., and Protasi, F. (2007). Reorganized stores and impaired calcium handling in skeletal muscle of mice lacking calsequestrin-1. J. Physiol. *583*, 767–784.

Pessah, I.N., Stambuk, R.A., and Casida, J.E. (1987). Ca^{2+}-activated ryanodine binding: mechanisms of sensitivity and intensity modulation by Mg^{2+}, caffeine, and adenine nucleotides. Mol. Pharmacol. *31*, 232–238.

Pollard, J.W., and Walker, J.M. (1997). Basic Cell Culture Protocols (Methods in Molecular Biology), Second Edition (Totowa, NJ: Humana Press).

Pou, S., Keaton, L., Surichamorn, W., and Rosen, G.M. (1999). Mechanism of superoxide generation by neuronal nitric-oxide synthase. J. Biol. Chem. *274*, 9573–9580.

Quane, K.A., Keating, K.E., Healy, J.M., Manning, B.M., Krivosic-Horber, R., Krivosic, I., Monnier, N., Lunardi, J., and McCarthy, T.V. (1994). Mutation screening of the RYR1 gene in malignant hypertherima: detection of a novel tyr to ser mutation in a pedigree with associated central core. Genomics *23*, 236–239.

Robertson, S. (1992). Advantages of etomidate use as an anesthetic agent. Vet. Clin. North Am. Small Anim. Pract. *22*, 277–280.

Rodney, G.G., Williams, B.Y., Strasburg, G.M., Beckingham, K., and Hamilton, S.L. (2000). Regulation of RYR1 activity by ca(2+) and calmodulin. Biochemistry *39*, 7807–7812.

Rossi, A.E., Boncompagni, S., Protasi, F., and Dirksen, R.T. (2006). Developmental regulation of mitochondrial triad targeting in skeletal muscle. Biophys. J. *90*, A269.

Ryan, J.F., and Tedeschi, L.G. (1997). Sudden unexplained death in a patient with a family history of malignant hyperthermia. J. Clin. Anesth. *9*, 66–68.

Sun, J., Xin, C., Eu, J.P., Stamler, J.S., and Meissner, G. (2001a). Cysteine-3635 is responsible for skeletal muscle ryanodine receptor modulation by no. Proc. Natl. Acad. Sci. USA *98*, 11158–11162.

Sun, J., Xu, L., Eu, J.P., Stamler, J.S., and Meissner, G. (2001b). Classes of thiols that influence the activity of the skeletal muscle calcium release channel. J. Biol. Chem. *276*, 15625–15630.

Sun, J., Xu, L., Eu, J.P., Stamler, J.S., and Meissner, G. (2003). Nitric oxide, noc-12, and s-nitrosoglutathione modulate the skeletal muscle calcium release channel/ryanodine receptor by different mechanisms. an allosteric function for o_2 in s-nitrosylation of the channel. J. Biol. Chem. *278*, 8184–8189.

Thompson, P.D., Franklin, B.A., Balady, G.J., Blair, S.N., Corrado, D., Estes, N.A., 3rd, Fulton, J.E., Gordon, N.F., Haskell, W.L., Link, M.S., et al. (2007). Exercise and acute cardiovascular events placing the risks into perspective: a scientific statement from the american heart association council on nutrition, physical activity, and metabolism and the council on clinical cardiology. Circulation *115*, 2358–2368.

Tietze, F. (1969). Enzymic method for quantitative determination of nanogram amounts of total and oxidized glutathione: applications to mammalian blood and other tissues. Anal. Biochem. *27*, 502–522.

Treves, S., Anderson, A.A., Ducreux, S., Divet, A., Bleunven, C., Grasso, C., Paesante, S., and Zorzato, F. (2005). Ryanodine receptor 1 mutations, dysregulation of calcium homeostasis and neuromuscular disorders. Neuromuscul. Disord. *15*, 577–587.

Wappler, F., Fiege, M., Steinfath, M., Agarwal, K., Scholz, J., Singh, S., Matschke, J., and Schulte Am Esch, J. (2001). Evidence for susceptibility to malignant hyperthermia in patients with exercise-induced rhabdomyolysis. Anesthesiology *94*, 95–100.

Wells, K.E., Torelli, S., Lu, Q., Brown, S.C., Partridge, T., Muntoni, F., and Wells, D.J. (2003). Relocalization of neuronal nitric oxide synthase (nNOS) as a marker for complete restoration of the dystrophin associated protein complex in skeletal muscle. Neuromuscul. Disord. *13*, 21–31.

Zhang, H., Zhang, J.Z., Danila, C.I., and Hamilton, S.L. (2003). A noncontiguous, inter-subunit binding site for calmodulin on the skeletal muscle Ca^{2+} release channel. J. Biol. Chem. *278*, 8348–8355.